OPTIMIZATION AND GAMMA/THETA GUIDANCE OF FLIGHT TRAJECTORIES IN A WINDSHEAR [1,2,3]

A. Miele[4], T. Wang[5], and W. W. Melvin[6]
Rice University, Houston, Texas
ALPA, Washington, DC

Abstract. This paper is concerned with guidance strategies for near-optimum performance in a windshear. The take-off problem is considered with reference to flight in a vertical plane. In addition to the horizontal shear, the presence of a downdraft is assumed.

First, trajectories for optimum performance in a windshear are determined for different windshear models and different windshear intensities. Use is made of the methods of optimal control theory in conjunction with the dual sequential gradient-restoration algorithm (DSGRA) for optimal control problems. In this approach, global information on the wind flow field is needed.

Then, guidance strategies for near-optimum performance in a windshear are developed, starting from the optimal trajectories. Specifically, three guidance schemes are presented: an absolute gamma guidance scheme, based on the absolute path inclination; a relative gamma guidance scheme, based on the relative path inclination; and a theta guidance scheme, based on the pitch attitude angle. In this approach, local information on the wind flow field is needed.

Numerical experiments show that the gamma/theta guidance schemes produce trajectories which are quite close to the optimum trajectories. In addition, the near-optimum trajectories are considerably superior to the trajectories arising from alternative guidance schemes.

An important characteristic of the gamma/theta guidance schemes is their simplicity. Indeed, these guidance schemes are implementable using available instrumentation and/or modification of available instrumentation.

Key Words. Guidance strategies, gamma guidance, theta guidance, flight mechanics, take-off, optimal trajectories, optimal control, feedback control, windshear problems, sequential gradient-restoration algorithm, dual sequential gradient-restoration algorithm.

1. Introduction

Low altitude windshear constitutes a considerable hazard in the take-off and landing of

---

[1] Paper presented at the 15th ICAS Congress, London, England, September 7-12, 1986 (Paper No. ICAS-86-564).

[2] This research was supported by NASA-Langley Research Center, Grant No. NAG-1-516, and by Boeing Commercial Aircraft Company.

[3] The authors are indebted to Dr. R. L. Bowles, NASA-Langley Research Center, for helpful discussions. The authors are also indebted to Mr. Z. G. Zhao and Mr. E. Kamaric, Rice University, for analytical and computational assistance.

[4] Professor of Astronautics and Mathematical Sciences, Aero-Astronautics Group, Rice University, Houston, Texas.

[5] Senior Research Associate, Aero-Astronautics Group, Rice University, Houston, Texas.

[6] Captain, Delta Airlines, Atlanta, Georgia; and Chairman, Airworthiness and Performance Committee, Air Line Pilots Association (ALPA), Washington, DC.

both civilian airplanes and military airplanes. For this reason, considerable research has been done on this problem over the past 15 years. Most of the research has been concerned with meteorology, instrumentation, aerodynamics, flight mechanics, and stability and control. Recently, optimal flight trajectories in the presence of a windshear have been studied (Refs. 1-3). This opens the road to the development of guidance schemes for achieving near-optimum performance in a windshear (Refs. 4-5).

Previous Research. Previous research on the topics covered in this paper can be found in Refs. 6-42. For a general review of windshear studies, see Ref. 6. For the equations of motion without windshear, see Ref. 7; for the equations of motion with windshear, see Refs. 8-11. For windshear models, see Refs. 12-16.

Concerning trajectory optimization, for a recent overview of theoretical calculus of variations and optimal control, see Ref. 17. For algorithmic optimal control by means of gradient methods, see Refs. 18-22 (primal formulation) and Refs. 23-24 (dual formulation). For minimax optimal control, see Refs. 25-37; in particular, for aerospace applications of minimax optimal control, see Refs. 26 and 33-37. Finally, for guidance schemes, see Refs. 4, 5, 16 and 38-42.

Present Research. This paper is concerned with guidance schemes for near-optimum performance in a windshear. In addition to the horizontal shear, the presence of a downdraft is assumed. Note that the downdraft had been neglected in Refs. 1-5.

The take-off problem is considered with reference to flight in a vertical plane. In take-off, once an aircraft becomes airborne, the pilot has no choice but to fly through a windshear. His only control is the angle of attack. Indeed, it is logical to assume that, if a plane takes off under less-than-ideal weather conditions, the power setting is being held at that value which yields the maximum thrust.

First, trajectories for optimum performance in a windshear are determined for different windshear models and different windshear intensities. Use is made of the methods of optimal control theory in conjunction with the dual sequential gradient-restoration algorithm (DSGRA) for optimal control problems. In this approach, global information on the wind flow field is needed.

Then, guidance schemes for near-optimum performance in a windshear are developed, starting from the optimal trajectories, specifically: gamma guidance, based on either the absolute or the relative path inclination; and theta guidance, based on the pitch attitude angle. In this approach, local information on the wind flow field is needed.

The gamma/theta guidance schemes are evaluated through numerical experiments (i) in order to determine whether the resulting trajectories are sufficiently close to the optimum trajectories and (ii) in order to compare the resulting trajectories with those arising from alternative guidance schemes. An important characteristic of the gamma/theta guidance schemes is their simplicity. Indeed, these guidance schemes are implementable using available instrumentation and/or modification of available instrumentation.

Outline. Section 2 contains the notations, and Section 3 contains the formulation of the problem. Section 4 pertains to optimum flight trajectories. Section 5 refers to the gamma/theta guidance schemes for near-optimum flight trajectories.

Finally, the conclusions are given in Section 6.

2. Notations

Throughout the paper, the following notations are employed:

ARL = aircraft reference line;

C_D = drag coefficient;

C_L = lift coefficient;

D = drag force, lb;

g = acceleration of gravity, ft sec^{-2};

E = energy per unit weight, ft;

h = altitude, ft;

K = gain coefficient;

L = lift force, lb;

m = mass, lb ft^{-1} sec^2;

S = reference surface, ft^2;

T = thrust force, lb;

V = relative velocity, ft sec^{-1};

V_e = absolute velocity, ft sec^{-1};

W = mg = weight, lb;

W = wind velocity, ft sec^{-1};

W_h = h-component of wind velocity, ft sec^{-1};

W_x = x-component of wind velocity, ft sec^{-1};

x = horizontal distance, ft.

Greek Symbols

α = relative angle of attack, rad;

α_e = absolute angle of attack, rad;

β = engine power setting;

γ = relative path inclination, rad;

γ_e = absolute path inclination, rad;

δ = thrust inclination, rad;

δ_e = elevator deflection, rad;

θ = pitch attitude angle, rad;

ρ = air density, lb ft^{-4} sec^2.

Subscripts

e = denotes Earth-fixed system;

ℓ = denotes direction orthogonal to relative velocity;

ℓe = denotes direction orthogonal to absolute velocity;

h = denotes h-direction;

x = denotes x-direction;

v = denotes direction of relative velocity;

ve = denotes direction of absolute velocity.

Superscripts

$\cdot$ = denotes derivative with respect to time;

$\rightarrow$ = denotes vector quantity;

$\sim$ denotes nominal value.

3. Formulation of the Problem

3.1. Coordinate Systems. In Ref. 1, three coordinate systems were considered: (i) the Earth-fixed system, (ii) the relative wind-axes system, and (iii) the absolute wind-axes system. It was assumed that flight takes place in a vertical plane.

Let $\vec{V}$ denote the velocity of the aircraft with respect to the airstream; let $\vec{W}$ denote the velocity of the airstream with respect to the Earth; and let $\vec{V}_e$ denote the velocity of the aircraft with respect to the Earth. With this understanding, the above coordinate systems are defined as follows (see Fig. 1):

(i) in the Earth-fixed system Oxh, the point O is fixed with respect to the Earth; the x-axis is horizontal, positive in the sense of the motion; and the h-axis is orthogonal to the x-axis, hence vertical, positive upward;

(ii) in the relative wind-axes system $Px_v y_\ell$, the point P moves together with the aircraft; the x_v-axis has the direction of the relative velocity vector $\vec{V}$; and the y_ℓ-axis is orthogonal to the x_v-axis;

(iii) in the absolute wind-axes system $Px_{ve}y_{\ell e}$, the point P moves together with the aircraft; the x_{ve}-axis has the direction of the absolute velocity vector $\vec{V}_e$; and the $y_{\ell e}$-axis is orthogonal to the

x_{ve}-axis.

3.2. Equations of Motion. In this paper, we make use of the relative wind-axes system in connection with the following assumptions: (a) the aircraft is a particle of constant mass; (b) flight takes place in a vertical plane; (c) Newton's law is valid in an Earth-fixed system; and (d) the wind flow field is steady.

With the above premises, the equations of motion are written as follows:

$$\dot{x} = V\cos\gamma + W_x, \tag{1a}$$

$$\dot{h} = V\sin\gamma + W_h, \tag{1b}$$

$$\dot{V} = (T/m)\cos(\alpha + \delta) - D/m - g\sin\gamma - (\dot{W}_x\cos\gamma + \dot{W}_h\sin\gamma), \tag{1c}$$

$$\dot{\gamma} = (T/mV)\sin(\alpha + \delta) + L/mV - (g/V)\cos\gamma + (1/V)(\dot{W}_x\sin\gamma - \dot{W}_h\cos\gamma). \tag{1d}$$

Because of assumption (d), the total derivatives of the wind velocity components and the corresponding partial derivatives satisfy the relations

$$\dot{W}_x = (\partial W_x/\partial x)(V\cos\gamma + W_x) + (\partial W_x/\partial h)(V\sin\gamma + W_h), \tag{2a}$$

$$\dot{W}_h = (\partial W_h/\partial x)(V\cos\gamma + W_x) + (\partial W_h/\partial h)(V\sin\gamma + W_h). \tag{2b}$$

As a consequence, the equations of motion can be rewritten in the form

$$\dot{x} = V\cos\gamma + W_x, \tag{3a}$$

$$\dot{h} = V\sin\gamma + W_h, \tag{3b}$$

$$\dot{V} = (T/m)\cos(\alpha + \delta) - D/m - g\sin\gamma - [(\partial W_x/\partial x)(V\cos\gamma + W_x) + (\partial W_x/\partial h)(V\sin\gamma + W_h)]\cos\gamma - [(\partial W_h/\partial x)(V\cos\gamma + W_x) + (\partial W_h/\partial h)(V\sin\gamma + W_h)]\sin\gamma, \tag{3c}$$

$$\dot{\gamma} = (T/mV)\sin(\alpha + \delta) + L/mV - (g/V)\cos\gamma + [(\partial W_x/\partial x)(V\cos\gamma + W_x) + (\partial W_x/\partial h)(V\sin\gamma + W_h)](1/V)\sin\gamma - [(\partial W_h/\partial x)(V\cos\gamma + W_x) + (\partial W_h/\partial h)(V\sin\gamma + W_h)](1/V)\cos\gamma. \tag{3d}$$

These equations must be supplemented by the functional relations

$$T = T(h,V,\beta), \tag{4a}$$

$$D = D(h,V,\alpha), \qquad L = L(h,V,\alpha), \tag{4b}$$

$$W_x = W_x(x,h), \qquad W_h = W_h(x,h), \tag{4c}$$

and by the analytical relations

$$V_{ex} = V\cos\gamma + W_x, \qquad W_{eh} = V\sin\gamma + W_h, \tag{5a}$$

$$V_e = \sqrt{(V_{ex}^2 + V_{eh}^2)}, \quad \gamma_e = \arctan(V_{eh}/V_{ex}), \tag{5b}$$

$$\theta = \alpha + \gamma, \qquad \alpha_e = \alpha + \gamma - \gamma_e. \tag{5c}$$

For a given value of the thrust inclination δ, the differential system (3)-(4) involves four state variables [the horizontal distance $x(t)$, the altitude $h(t)$, the velocity $V(t)$, and the relative path inclination $\gamma(t)$] and two control variables [the angle of attack $\alpha(t)$ and the power setting $\beta(t)$]. However, the number of control variables reduces to one (the angle of attack α), if the power setting β is specified in advance. The quantities defined by the analytical relations (5) can be computed a posteriori, once the values of $x,h,V,\gamma,\alpha,\beta$ are known.

3.3. Inequality Constraints. The angle of attack α and its time derivative $\dot{\alpha}$ are subject to the inequalities

$$\alpha \leq \alpha_*, \tag{6a}$$

$$-C \leq \dot{\alpha} \leq +C, \tag{6b}$$

where α_* is a prescribed upper bound and ϵ is a prescribed, positive constant.

For the optimal trajectories of Section 4, Ineqs. (6) are satisfied indirectly via transformation techniques converting the inequality constraints into equality constaints (see Ref. 1, Part 2), specifically,

$$\alpha = \alpha_* - u^2, \tag{7a}$$

$$\dot{u} = -(C/2u)\sin w, \qquad |u| \geq \varepsilon, \tag{7b}$$

$$\dot{u} = -(C/2u)\sin^2(\pi u/2\varepsilon)\sin w, \qquad |u| \leq \varepsilon. \tag{7c}$$

Here, $u(t)$, $w(t)$ are auxiliary variables and ε is a small, positive constant, which is introduced to prevent the occurrence of singularities. Incidentally, the right-hand sides of Eqs. (7b)-(7c) are continuous and have continuous first derivatives at $|u| = \varepsilon$.

For the guidance schemes of Section 5, Ineq. (6a) is satisfied directly. On the other hand, Ineq. (6b) is satisfied indirectly through the proper choice of the gain coefficient K.

3.4. Approximations for the Force Terms. In this section, we discuss the approximations employed in the description of the forces acting on the aircraft, namely, the thrust, the drag, the lift, and the weight. Because the trajectories under investigation involve relatively minor variations of the altitude, the air density is assumed to be constant.

Thrust. The thrust T is approximated with the quadratic function

$$T = A_0 + A_1 V + A_2 V^2, \tag{8}$$

where V is the relative velocity. The coefficients A_0, A_1, A_2 depend on the altitude of the runway, the ambient temperature, and the engine power setting; they can be determined with a least-square fit of manufacturer-supplied data over a given interval of velocities.

Drag. The drag D is written in the form

$$D = (1/2)C_D \rho S V^2, \tag{9a}$$

$$C_D = B_0 + B_1\alpha + B_2\alpha^2, \qquad \alpha \leq \alpha_*, \tag{9b}$$

where ρ is the air density, S is a reference surface, V is the relative velocity, and C_D is the drag coefficient. The coefficients B_0, B_1, B_2 depend on the flap setting and the undercarriage position (gear up or gear down); they can be determined with a least-square fit of manufacturer-supplied data over the interval $0 \leq \alpha \leq \alpha_*$.

Lift. The lift L is written in the form

$$L = (1/2)C_L \rho S V^2, \tag{10a}$$

$$C_L = C_0 + C_1\alpha, \qquad \alpha \leq \alpha_{**}, \tag{10b}$$

$$C_L = C_0 + C_1\alpha + C_2(\alpha - \alpha_{**})^2, \qquad \alpha_{**} \leq \alpha \leq \alpha_*, \tag{10c}$$

where ρ is the air density, S is a reference surface, V is the relative velocity, and C_L is the lift coefficient. The coefficients C_0, C_1, C_2 depend on the flap setting and the undercarriage position (gear up or gear down); they can be determined with a least-square fit of manufacturer-supplied data over the intervals $0 \leq \alpha \leq \alpha_{**}$ and $\alpha_{**} \leq \alpha \leq \alpha_*$.

Weight. The mass m is regarded to be constant. Hence, the weight $W = mg$ is regarded to be constant.

3.5. Approximations for the Windshear. In this section, we discuss some of the approximations employed in the description of the windshear. We observe that, under the assumption that the wind flow field is steady, the wind components W_x, W_h have the form

$$W_x = W_x(x,h), \qquad W_h = W_h(x,h). \tag{11}$$

Windshear Models. Over the past several years, considerable attention has been given to the study

of a severe meteorological condition known as a microburst (Refs. 6 and 8-16). This condition involves a descending column of air, which then spreads horizontally in the neighborhood of the ground. This condition is hazardous, because an aircraft in take-off or landing might encounter a headwind coupled with a downdraft, followed by a tailwind coupled with a downdraft. A qualitative example of the vertical cross section of a microburst is shown in Fig. 2.

It is clear that, in order to perform realistic analyses of take-off and landing under severe meteorological conditions, one must represent wind flow fields of the type shown in Fig. 2. The representation of the wind flow field can be obtained from the combination of theory and experimental measurements.

From an engineering point of view, a simplifying observation can be made. Because take-off trajectories involve relatively minor variations of the altitude, the wind components W_x, W_h can be assumed to depend only on the horizontal distance. Within this frame, three different windshear models are of interest:

$$(WS1) \quad W_x = W_x(x), \quad W_h = 0; \tag{12a}$$

$$(WS2) \quad W_x = 0, \quad W_h = W_h(x); \tag{12b}$$

$$(WS3) \quad W_x = W_x(x), \quad W_h = W_h(x). \tag{12c}$$

Windshear model WS1 includes the horizontal shear and neglects the downdraft; this is the model considered in Refs. 1-5; windshear model WS2 is complementary to WS1, in that it neglects the horizontal shear and includes the downdraft; finally, windshear model WS3 generalizes WS1 and WS2, in that it includes both the horizontal shear and the downdraft.

The study of the optimal trajectories and associated guidance schemes for each of these windshear models is essential to build a qualitative understanding of how an aircraft must fly in a microburst; it is also essential to construct either automatic or semi-automatic guidance schemes which are robust, that is, capable of functioning under a variety of operating conditions.

4. Optimal Flight Trajectories

4.1. Optimal Control Problem. We refer to take-off trajectories and we assume that: (i) the aircraft is airborne; (ii) global information on the wind flow field is available, that is, the functions (4c) are known in advance; (iii) the power setting $\beta(t)$ is given; and (iv) the angle of attack $\alpha(t)$ is subject to Ineqs. (6). Hence, upon converting the inequalities into equalities, we refer to the differential system described by Eqs. (3), (4), (7). In this system, the state variables are $x(t)$, $h(t)$, $V(t)$, $\gamma(t)$, $\alpha(t)$, $u(t)$ and the control variable is $w(t)$. In accordance with the terminology employed in Refs. 1-5, we formulate the following optimization problem.

Problem (P8). Minimize the peak value of the modulus of the difference between the absolute path inclination and a reference value, assumed constant. In this problem, the performance index is given by

$$I = \max_t |\gamma_e - \gamma_{eR}|, \qquad 0 \leq t \leq \tau, \tag{13a}$$

where

$$\gamma_e = \arctan[(V\sin\gamma + W_h)/(V\cos\gamma + W_x)], \tag{13b}$$

$$\gamma_{eR} = \gamma_{e0}. \tag{13c}$$

This is a minimax problem or Chebyshev problem of optimal control. It can be reformulated as a Bolza problem of optimal control (Ref. 37), in

which one minimizes the integral performance index

$$J = \int_0^\tau (\gamma_e - \gamma_{eR})^q dt, \tag{13d}$$

for large values of the positive, even exponent q.

4.2. Boundary Conditions. Concerning the initial conditions, it is assumed that the values of x,h,V,γ,α are specified at $t = 0$, that is,

$$x(0) = x_0, \qquad h(0) = h_0, \qquad V(0) = V_0, \tag{14a}$$

$$\gamma(0) = \gamma_0, \qquad \alpha(0) = \alpha_0. \tag{14b}$$

Upon combining (7a) and (14b), we see that the specification of the initial value of α implies the specification of the initial value of u, that is,

$$u(0) = u_0 = \sqrt{(\alpha_* - \alpha_0)}. \tag{14c}$$

Concerning the final conditions, it is assumed that the value of γ is specified at $t = \tau$, that is,

$$\gamma(\tau) = \gamma_0. \tag{15}$$

The remaining state variables are free at the final point. The final time τ is chosen to be large enough to correspond to a no-windshear condition.

Clearly, use of (15) means that, at the final point, one intends to restore the initial value of the relative path inclination. In accordance with the terminology employed in Refs. 1-5, this type of boundary condition is called boundary condition BC1.

4.3. Sequential Gradient-Restoration Algorithm. Problem (P8), governed by Eqs. (3)-(4), (7), (13)-(15), is a Bolza problem of optimal control. It can be solved using the family of sequential gradient-restoration algorithms for optimal control problems (SGRA, Refs. 18-24), in either the primal formulation (PSGRA, Refs. 18-22) or the dual formulation (DSGRA, Refs. 23-24).

Regardless of whether the primal formulation is used or the dual formulation is used, sequential gradient-restoration algorithms involve a sequence of two-phase cycles, each cycle including a gradient phase and a restoration phase. In the gradient phase, the value of the augmented functional is decreased, while avoiding excessive constraint violation. In the restoration phase, the value of the constraint error is decreased, while avoiding excessive change in the value of the functional. In a complete gradient-restoration cycle, the value of the functional is decreased, while the constraints are satisfied to a preselected degree of accuracy. Thus, a succession of suboptimal solutions is generated, each new solution being an improvement over the previous one from the point of view of the value of the functional being minimized.

The convergence conditions are represented by the relations

$$P \leq \varepsilon_1, \qquad Q \leq \varepsilon_2. \tag{16}$$

Here, P is the norm squared of the error in the constraints (3)-(4), (7), (14)-(15); Q is the norm squared of the error in the optimality conditions; and ε_1, ε_2 are preselected, small, positive numbers.

In this work, the sequential gradient-restoration algorithm is employed in conjunction with the dual formulation. The algorithmic details can be found in Ref. 1, Part 3. They are omitted here, for the sake of brevity.

4.4. Data for the Examples. In this section, we present the data used in the numerical experiments.

Aircraft. The aircraft under consideration is a Boeing B-727 aircraft powered by three JT8D-17 turbofan engines. It is assumed that: (i)

the aircraft has become airborne from a runway located at sea-level altitude; (ii) the ambient temperature is 100 deg Fahrenheit; (iii) the gear is up; (iv) the flap setting is δ_F = 15 deg; (v) the engines are operating at maximum power setting; and (vi) the take-off weight is W = 180,000 lb.

Complete data for this aircraft are omitted here, for the sake of brevity; they can be found in Ref. 1, Part 4. It is of interest to note that the maximum lift-to-drag ratio of this configuration is $(L/D)_{max}$ = 10.52 and that the average thrust-to-weight ratio over the velocity interval $200 \leq V \leq 300$ ft sec^{-1} is $(T/W)_{av}$ = 0.22.

Windshear Models. Three windshear models are considered. They are described by Eqs. (12) and are shown in Fig. 3.

Model WS1. This model has the form (12a); it includes the horizontal shear and neglects the downdraft. The function $W_x(x)$ represents a linear transition from a uniform headwind of -40 ft sec^{-1} to a uniform tailwind of +40 ft sec^{-1}; hence, the wind velocity difference is ΔW_x = 80 ft sec^{-1}. The transition takes place over a distance Δx = 4,000 ft, starting at x = 300 ft and ending at x = 4,300 ft; hence, the average wind gradient is $\Delta W_x/\Delta x$ = 0.020 sec^{-1}.

Model WS2. This model has the form (12b); it is complementary to model WS1, in that it neglects the horizontal shear and includes the downdraft. The function $W_h(x)$ has a bell-shaped form; in particular, the downdraft vanishes at x = 300 ft and x = 4,300 ft and achieves the maximum negative value of -20 ft sec^{-1} at x = 2,300 ft; hence, ΔW_h = 20 ft sec^{-1}.

Model WS3. This model has the form (12c); it generalizes models WS1 and WS2, in that it includes both the horizontal shear and the downdraft. The function $W_x(x)$ is the same as in model WS1; the function $W_h(x)$ is the same as in model WS2.

The assumed wind models are smoothed in such a way that the continuity of the functions, the first derivatives, and the second derivatives is assured; for details of the smoothing procedure, see Ref. 1, Part 2.

Inequality Constraints. The angle of attack and its time derivative are subject to Ineqs. (6), with

$$\alpha_* = 16 \text{ deg}, \qquad C = 3 \text{ deg sec}^{-1}. \tag{17}$$

The constant ε in Eqs. (7) is set at the level

$$\varepsilon = 0.4. \tag{18}$$

Initial Conditions. The following initial conditions are assumed:

$$x(0) = 0 \text{ ft}, \qquad h(0) = 50 \text{ ft}, \tag{19a}$$

$$V(0) = 276.8 \text{ ft sec}^{-1}, \qquad \gamma(0) = 6.989 \text{ deg}, \tag{19b}$$

$$\alpha(0) = 10.36 \text{ deg}. \tag{19c}$$

We note that the initial velocity is FAA certification velocity V_2, augmented by 10 knots. In turn, the velocity V_2 + 10 (in knots) corresponds approximately to the steepest climb condition in quasi-steady flight.

Final Conditions. In boundary condition model BC1, it is required that

$$\gamma(\tau) = 6.989 \text{ deg}. \tag{20}$$

The final time is set at the value

$$\tau = 40 \text{ sec}. \tag{21}$$

This is about twice the duration of the windshear encounter (Δt = 18 sec).

Performance Index. The numerical constants appearing in the performance indexes I and J of Problem (P8) are given below:

γ_{eR} = 8.165 deg, q = 6. (22)

4.5. Numerical Results. Problem (P8), minimax $|\Delta\gamma_e|$, was solved in connection with boundary condition model BC1. The sequential gradient-restoration algorithm was employed in conjunction with the dual formulation (DSGRA, Refs. 23-24). This algorithm was programmed in FORTRAN IV, and the numerical results were obtained in double-precision arithmetic. Computations were performed at Rice University using an NAS-AS-9000 computer.

The interval of integration was divided into 100 steps. The differential systems were integrated using Hamming's modified predictor-corrector method, with a special Runge-Kutta starting procedure. Definite integrals were computed using a modified Simpson's rule. Linear algebraic systems were solved using a standard Gaussian elimination routine.

Windshear models WS1, WS2, WS3 were considered. Alternative windshear models were generated by changing the windshear intensities (hence, the values of ΔW_x, ΔW_h) and by subsequent proportional scaling of the functions $W_x(x)$, $W_h(x)$. However, for the sake of brevity, we limit our presentation to models WS1, WS2, WS3. We recall that these models are characterized by the following values of ΔW_x, ΔW_h:

(WS1) ΔW_x = 80 ft sec^{-1}, ΔW_h = 0 ft sec^{-1}; (23a)

(WS2) ΔW_x = 0 ft sec^{-1}, ΔW_h = 20 ft sec^{-1}; (23b)

(WS3) ΔW_x = 80 ft sec^{-1}, ΔW_h = 20 ft sec^{-1}. (23c)

For computational efficiency, the state variables and the time were suitably scaled. For Problem (P8), the functional being minimized was suitably scaled. The following stopping conditions were employed for the dual sequential gradient-restoration algorithm:

$P \leq$ E-10, $Q \leq$ E-08, (24)

where P denotes the constraint error and Q denotes the error in the optimality conditions.

The results are given in Fig. 4, which contains eight parts: the wind velocity components W_x, W_h; the flight altitude h; the relative velocity V; the relative path inclination γ; the relative angle of attack α; the pitch attitude angle θ; the absolute path inclination γ_e; and the energy per unit weight $E = h + V^2/2g$. The following comments are pertinent.

Altitude. For all the optimal trajectories, the altitude distribution h(t) exhibits a monotonic behavior, regardless of the windshear model. For model WS2, the function h(t) is almost identical with that characterizing the nominal trajectory in the absence of downdraft. This means that $\gamma_e \cong \gamma_{e0}$, a condition which can be achieved by properly adjusting the angle of attack $\alpha(t)$.

For model WS3, there is large time interval, approximately Δt = 18 sec, in which the optimal trajectory is nearly horizontal ($\gamma_e \cong 0$); this is due to the combined effect of the horizontal shear and the downdraft; after passing through the shear region, the aircraft resumes climbing.
For model WS1, the function h(t) is intermediate between that of model WS2 and that of model WS3, being closer to the latter than to the former.

Angle of Attack. For model WS2, a gradual, moderate change in the angle of attack is required in order to compensate for the downdraft. However, the angle of attack boundary is never reached. This is why, by properly adjusting the angle of attack distribution $\alpha(t)$, one can obtain an optimal trajectory close to the nominal trajectory in the absence of downdraft.

For models WS1 and WS3, an initial decrease in the angle of attack is needed, followed by a gradual, sustained increase until the angle of attack boundary is reached. This occurs at about the time when the shear end (t = 18 sec). Afterward, the angle of attack is kept at the maximum permissible value for a relatively long time interval (Δt = 10 sec). As a consequence, for both models WS1 and WS3, the optimal trajectory departs to a considerable extent from the nominal trajectory.

It is interesting to note that the angle of attack distributions of models WS1 and WS3 are nearly the same, which means that the control action is mostly determined by the horizontal shear. This also means that the effect of the downdraft is mostly kinematical, rather than dynamical: the function $h(t)$ for model WS3 is shifted downward with respect to that for model WS1.

Absolute Path Inclination. For model WS2, the optimal trajectory is such that $\gamma_e \cong \gamma_{e0}$. Hence, the performance index of Problem (P8), minimax $|\Delta\gamma_e|$, is nearly zero.

For models WS1 and WS3, the behavior of γ_e is quite different. Initially, γ_e must be decreased until a certain critical value $\gamma_e = \gamma_{ec}$ is reached; then, this value is nearly maintained for a relatively long time interval (Δt = 24 sec for model WS1 and Δt = 18 sec for model WS3). After passing through the shear region, the value of γ_e is gradually increased to $\gamma_e \cong \gamma_{e0}$.

The critical value of the absolute path inclination is of interest in constructing a guidance algorithm. From the inspection of the optimal trajectories, we see that $\gamma_{ec}/\gamma_{e0} \cong 1$ for model WS2, $\gamma_{ec}/\gamma_{e0} \cong 0.4$ for model WS1, and $\gamma_{ec}/\gamma_{e0} \cong 0$ for model WS3.

Relative Path Inclination. For model WS1, the relative path inclination γ behaves in about the same way as the absolute path inclination γ_e. This is due to the absence of downdraft.

For models WS2 and WS3, the relative path inclination γ is larger than the absolute path inclination γ_e. This is in order to compensate for the presence of downdraft.

Relative Velocity. For model WS2, there is a mild decrease in relative velocity, consistent with the increase in the angle of attack. The velocity decrease ends at about the time when the downdraft ends.

For models WS1 and WS3, there is a stronger decrease in relative velocity. The maximum drop in relative velocity depends mainly on the wind velocity difference ΔW_x and occurs at about the time when the shear ends (t = 18 sec).

4.6. Comment. From the present study of optimal trajectories (Fig. 4) as well as from previous studies (Refs. 1-3), the following conclusions can be inferred. For weak-to-moderate shear/downdraft combinations, the optimal trajectory is characterized by a monotonic climb. For severe shear/downdraft combinations, the optimal trajectory is characterized by an initial climb, followed by nearly-horizontal flight, followed by renewed climbing after the aircraft has passed through the shear region.

5. Gamma/Theta Guidance

This section pertains to guidance schemes for near-optimum flight trajectories. First we introduce a gamma guidance scheme, based on the absolute path inclination γ_e. Because it might be

difficult to measure γ_e, we then convert the absolute gamma guidance scheme into the relative gamma guidance scheme, which is based on γ. Finally, we introduce the theta guidance scheme, based on the pitch attitude angle θ.

5.1. Absolute Gamma Guidance. This guidance scheme is based on certain basic facts, which can be established by inspection of the optimal trajectories presented in Fig. 4:

(i) initially, γ_e must be decreased until a certain critical value is reached; the critical value of γ_e is nearly maintained for a relatively long time interval; after passing through the shear region, the value of γ_e is gradually increased to $\gamma_e \cong \gamma_{e0}$;

(ii) the critical value of γ_e depends on the intensity of the shear $\dot{W}_x/g$ and the intensity of the downdraft W_h/V; it decreases as the intensities of the shear and the downdraft increase.

From facts (i) and (ii), as well as from previous work on optimal trajectories and guidance schemes in the absence of downdraft (Refs. 1-5), we surmise that the absolute gamma guidance law should have the form

$$\gamma_e = \tilde{\gamma}_e(\dot{W}_x/g,\ W_h/V), \tag{25}$$

where

$$\tilde{\gamma}_e = A[1 - B(\dot{W}_x/g)] + B(\dot{W}_x/g)(W_h/V),$$

$$\tilde{\gamma}_{e1} \leq \tilde{\gamma}_e \leq \tilde{\gamma}_{e2}. \tag{26}$$

Here, A, B are suitable constants, to be derived from the study of the optimal trajectories; and $\tilde{\gamma}_{e1}$, $\tilde{\gamma}_{e2}$ are specified lower and upper bounds to the absolute path inclination.

Alternatively, providing γ_e can be measured, Eq. (25) can be implemented through the feedback control law

$$\alpha - \tilde{\alpha}(V) = -K[\gamma_e - \tilde{\gamma}_e(\dot{W}_x/g, W_h/V)], \qquad \alpha \leq \alpha_*, \tag{27}$$

where K is the gain coefficient. In Eq. (27), $\tilde{\alpha}(V)$ denotes the nominal angle of attack, whose structure is discussed in Section 5.4, and $\tilde{\gamma}_e(\dot{W}_x/g,\ W_h/V)$ denotes the nominal absolute path inclination, which is supplied by (26).

5.2. Relative Gamma Guidance. Because it might be difficult to measure γ_e, we convert the absolute gamma guidance scheme into the relative gamma guidance scheme, which is based on γ. We observe that the following relation exists between the absolute and relative path inclinations [see (5a), (5b)]:

$$\tan\gamma_e = (V\sin\gamma + W_h)/(V\cos\gamma + W_x). \tag{28}$$

If one assumes that

$$\tan\gamma_e \cong \gamma_e, \tag{29a}$$

$$\cos\gamma \cong 1, \qquad \sin\gamma \cong \gamma, \tag{29b}$$

$$|W_x/V| << 1, \tag{29c}$$

Eq. (28) reduces to

$$\gamma_e = \gamma + W_h/V, \tag{30a}$$

with the implication that

$$\tilde{\gamma}_e = \tilde{\gamma} + W_h/V. \tag{30b}$$

Upon combining (25)-(26) with (30), we deduce that the relative gamma guidance law should have the form

$$\gamma = \tilde{\gamma}(\dot{W}_x/g,\ W_h/V), \tag{31}$$

where

$$\tilde{\gamma} = (A - W_h/V)[1 - B(\dot{W}_x/g)], \qquad \tilde{\gamma}_1 \leq \tilde{\gamma} \leq \tilde{\gamma}_2, \tag{32a}$$

with

$$\tilde{\gamma}_1 = \tilde{\gamma}_{e1} - W_h/V, \tag{32b}$$

$$\tilde{\gamma}_2 = \tilde{\gamma}_{e2} - W_h/V. \tag{32c}$$

Alternatively, Eq. (32a) can be implemented through the feedback control law

$$\alpha - \tilde{\alpha}(V) = -K[\gamma - \tilde{\gamma}(\dot{W}_x/g,\ W_h/V)], \qquad \alpha \leq \alpha_*, \quad (33)$$

where K is the gain coefficient. In Eq. (33), $\tilde{\alpha}(V)$ denotes the nominal angle of attack, whose structure is discussed in Section 5.4, and $\tilde{\gamma}(\dot{W}_x/g,\ W_h/V)$ denotes the nominal relative path inclination, which is supplied by (32).

5.3. Theta Guidance. An alternative to the gamma guidance scheme is the theta guidance scheme, based on the pitch attitude angle θ. We recall the first of Eqs. (5c),

$$\theta = \alpha + \gamma, \quad (34a)$$

with the implication that

$$\tilde{\theta} = \tilde{\alpha} + \tilde{\gamma}. \quad (34b)$$

Upon combining (31)-(32) with (34), and upon recalling that $\tilde{\alpha} = \tilde{\alpha}(V)$, we deduce that the theta guidance law should have the form

$$\theta = \tilde{\theta}(\dot{W}_x/g,\ W_h/V, V), \quad (35)$$

where

$$\tilde{\theta} = \tilde{\alpha}(V) + (A - W_h/V)[1 - B(\dot{W}_x/g)],$$

$$\tilde{\theta}_1 \leq \tilde{\theta} \leq \tilde{\theta}_2, \quad (36a)$$

with

$$\tilde{\theta}_1 = \tilde{\alpha}(V) + \tilde{\gamma}_{e1} - W_h/V, \quad (36b)$$

$$\tilde{\theta}_2 = \tilde{\alpha}(V) + \tilde{\gamma}_{e2} - W_h/V. \quad (36c)$$

Note that (34a) and (35) imply that

$$\alpha = \tilde{\theta}(\dot{W}_x/g,\ W_h/V, V) - \gamma, \qquad \alpha \leq \alpha_*. \quad (37)$$

Here, the nominal pitch attitude angle $\tilde{\theta}(\dot{W}_x/g,\ W_h/V, V)$ is supplied by (36).

Alternatively, Eq. (35) can be implemented through the feedback control law

$$\alpha - \tilde{\alpha}(V) = -K[\theta - \tilde{\theta}(\dot{W}_x/g,\ W_h/V, V)], \qquad \alpha \leq \alpha_*, \quad (38)$$

where K is the gain coefficient. In Eq. (38), $\tilde{\alpha}(V)$ denotes the nominal angle of attack, whose structure is discussed in Section 5.4, and $\tilde{\theta}(\dot{W}_x/g,\ W_h/V, V)$ denotes the nominal pitch attitude angle, which is supplied by (36).

5.4. Nominal Angle of Attack. From the analysis of the optimal trajectories of Fig. 4, it appears that there is some relation between the angle of attack and the velocity; it also appears that this relation is relatively insensitive to the windshear model and the windshear intensity; more specifically, low angles of attack correspond to high velocities, and high angles of attack correspond to low velocities. An analytical form for the function $\tilde{\alpha}(V)$ is derived below.

Recall Eq. (1d), and assume that, along a large portion of the optimal trajectory,

$$\cos\gamma \cong 1, \qquad \sin\gamma \cong \gamma, \quad (39a)$$

$$|\dot{W}_x\gamma/g| \ll 1, \quad |\dot{W}_h/g| \ll 1, \quad |V\dot{\gamma}/g| \ll 1. \quad (39b)$$

Under these conditions, Eq. (1d) yields the following nondifferential equation:

$$(T/W)\sin(\alpha + \delta) + L/W - 1 = 0, \quad (40)$$

which supplies implicitly the function $\tilde{\alpha}(V)$.

Next, we employ the representation (8) for the thrust and the representation (10) for the lift, namely,

$$T = A_0 + A_1 V + A_2 V^2, \quad (41a)$$

$$L = (1/2)(C_0 + C_1\alpha)\rho S V^2, \qquad \alpha \leq \alpha_{**}, \quad (41b)$$

$$L = (1/2)[C_0 + C_1\alpha + C_2(\alpha - \alpha_{**})^2]\rho S V^2,$$

$$\alpha_{**} \leq \alpha \leq \alpha_*, \quad (41c)$$

Also, we expand the trigonometric term $\sin(\alpha + \delta)$ in Taylor series as follows:

$$\sin(\alpha + \delta) \cong (\alpha + \delta). \quad (42)$$

From (40)-(42), we obtain the following algebraic equations:

$$D_0 + D_1\alpha = 0, \qquad \alpha \le \alpha_{**}, \quad (43a)$$

$$E_0 + E_1(\alpha - \alpha_{**}) + E_2(\alpha - \alpha_{**})^2 = 0, \qquad \alpha_{**} \le \alpha \le \alpha_*, \quad (43b)$$

which admit the solutions

$$\alpha = -D_0/D_1, \qquad \alpha \le \alpha_{**}, \quad (44a)$$

$$\alpha = \alpha_{**} + (1/2E_2)[-E_1 + \sqrt{(E_1^2 - 4E_0E_2)}], \qquad \alpha_{**} \le \alpha \le \alpha_*. \quad (44b)$$

The coefficients D_0, D_1 and E_0, E_1, E_2 depend on the velocity. They are given by

$$D_0 = -1 + (\delta/mg)(A_0 + A_1V + A_2V^2) + (C_0\rho S/2mg)V^2, \quad (45a)$$

$$D_1 = (1/mg)(A_0 + A_1V + A_2V^2) + (C_1\rho S/2mg)V^2, \quad (45b)$$

and

$$E_0 = D_0 + D_1\alpha_{**}, \quad (46a)$$

$$E_1 = D_1, \quad (46b)$$

$$E_2 = (C_2\rho S/2mg)V^2. \quad (46c)$$

Equations (44), in conjunction with Eqs. (45)-(46), supply explicitly the function $\tilde{\alpha}(V)$.

5.5. Implementation. The practical implementation of the gamma/theta guidance schemes requires the determination of the values V, γ, θ, α as well as the values of $\dot{h}$, $\dot{V}$ and $\dot{W}_x$, W_h, γ_e.

The state variables V, γ and the control variables θ, α can be measured with present instrumentation. An analogous remark holds for the rate of climb $\dot{h}$. The derivative $\dot{V}$ can be obtained by differentiation of the measured relative velocity V with respect to the time t. The values of $\dot{W}_x$, W_h, γ_e cannot be determined directly; they must be determined indirectly with the procedure below.

Computation of $\dot{W}_x$. Consider Eq. (1a) and observe that its time derivative is given by

$$\ddot{x} = \dot{V}\cos\gamma - V\sin\gamma\dot{\gamma} + \dot{W}_x. \quad (47)$$

If one assumes that

$$\cos\gamma \cong 1, \qquad \sin\gamma \cong \gamma, \quad (48a)$$

$$|V\gamma\dot{\gamma}/\dot{V}| << 1, \quad (48b)$$

Eq. (47) reduces to

$$\dot{W}_x = \ddot{x} - \dot{V}. \quad (49)$$

In turn, $\ddot{x}$ can be obtained from the measurement of the inertial acceleration, while $\dot{V}$ can be obtained by taking the time derivative of the relative velocity.

Computation of W_h. Consider Eq. (1b) and rewrite it in the form

$$W_h = \dot{h} - V\sin\gamma. \quad (50)$$

This enables one to compute the downdraft W_h, once the values of $V,\gamma,\dot{h}$ are known. They can be measured with present instrumentation.

Computation of γ_e. Consider Eq. (28) and make use of the approximations (29). This leads to the relation

$$\gamma_e = \gamma + W_h/V, \quad (51)$$

which enables one to compute γ_e, once the values of V,γ,W_h are known.

Alternatively, combine Eqs. (1b), (28) and make use of the approximations (29a), (29c). This leads to the relation

$$\gamma_e = \dot{h}/V, \quad (52)$$

which enables one to compute γ_e, once the values of $V,\dot{h}$ are known.

5.6. Elevator Deflection. In the previous sections, the gamma/theta guidance schemes were expressed in the feedback control forms (27), (33), (38). Because the rotational motion of the aircraft is not considered in this paper, the angle of attack α is the control variable.

If the rotational motion is considered, the elevator deflection δ_e replaces the angle of attack α as the control variable. As a consequence, the feedback control laws take the following more practical forms:

$$\delta_e - \tilde{\delta}_e = -K[\gamma_e - \tilde{\gamma}_e(\dot{W}_x/g, W_h/V)], |\delta_e| \leq \delta_{e*}, \quad (53a)$$

$$\delta_e - \tilde{\delta}_e = -K[\gamma - \tilde{\gamma}(\dot{W}_x/g, W_h/V)], \quad |\delta_e| \leq \delta_{e*}, \quad (53b)$$

$$\delta_e - \tilde{\delta}_e = -K[\theta - \tilde{\theta}(\dot{W}_x/g, W_h/V, V)], \quad |\delta_e| \leq \delta_{e*}, \quad (53c)$$

where $\tilde{\delta}_e$ is the nominal elevator deflection and δ_{e*} is the upper bound to the elevator deflection. We note that $\tilde{\delta}_e$ is a function of the state variables, to be suitably defined.

5.7. Numerical Results. The gamma/theta guidance schemes were programmed in FORTRAN IV, and the numerical results were obtained in double-precision arithmetic. Computations were performed at Rice University using an NAS-AS-9000 computer.

The interval of integration was divided into 500 steps. The differential system (3) was integrated using Hamming's modified predictor-corrector method with a special Runge-Kutta starting procedure.

The data for the examples are the same as those of Section 4.4. In particular, the initial conditions are given by Eqs. (19a), (19b) and the final time is given by Eq.(21). The angle of attack is subject to Ineq. (6a), with $\alpha_* = 16$ deg.

Windshear models WS1, WS2, WS3 were considered. Alternative windshear models were generated by changing the windshear intensities (hence, the values of ΔW_x, ΔW_h) and by subsequent proportional scaling of the functions $W_x(x)$, $W_h(x)$. However, for the sake of brevity, we limit our presentation to models WS1, WS2, WS3. We recall that these models are characterized by the values (23) for ΔW_x, ΔW_h.

The gamma/theta guidance schemes were implemented using the feedback control laws (27), (33), (38), with K = 10. However, for the sake of brevity, the computations presented here refer only to the relative gamma guidance scheme. Consistent results were obtained with the remaining schemes.

In implementing the relative gamma guidance scheme, the numerical constants appearing in Eqs. (32)-(33) were set at the following levels:

$$A = \gamma_0 = 0.1220 \text{ rad}, \quad B = 4, \quad (54a)$$

$$\tilde{\gamma}_{e1} = 0.0087 \text{ rad}, \ \tilde{\gamma}_{e2} = \gamma_0 = 0.1220 \text{ rad}. \quad (54b)$$

The results are given in Fig. 5, which contains eight parts: the wind velocity components W_x, W_h; the flight altitude h; the relative velocity V; the relative path inclination γ; the relative angle of attack α; the pitch attitude angle θ; the absolute path inclination γ_e; and the energy per unit weight $E = h + V^2/2g$.

Comparison of Figs. 4 and 5 shows that there is a remarkable qualitative agreement between the gamma guidance trajectories and the optimal trajectories. In particular, the following points must be noted.

Altitude. For model WS2, the function h(t) of the gamma guidance trajectory (GGT) is almost identical with the function h(t) characterizing

the nominal trajectory in the absence of downdraft; therefore, it behaves as the function h(t) of the optimal trajectory (OT).

For model WS3, there is a large time interval in which the function h(t) of the GGT is nearly constant. For model WS1, the function h(t) of the GGT is intermediate between that of model WS2 and that of model WS3, being closer to the latter than to the former; therefore, it behaves as the function h(t) of the OT.

Angle of Attack. For model WS2, the GGT exhibits a gradual, moderate change in the angle of attack; the angle of attack boundary is never reached; hence, the function $\alpha(t)$ of the GGT behaves as the function $\alpha(t)$ of the OT.

For models WS1 and WS3, the GGT exhibits an initial decrease in the angle of attack, followed by a gradual, sustained increase; the angle of attack boundary is reached at about the time when the shear ends; once more, the function $\alpha(t)$ of the GGT behaves as the function $\alpha(t)$ of the OT.

Absolute Path Inclination. For model WS2, the GGT is such that $\gamma_e \cong \gamma_{e0}$; this property is consistent with the analogous property of the OT.

For models WS1 and WS3, the absolute path inclination γ_e of the GGT decreases until a certain critical value $\gamma_e = \gamma_{ec}$ is reached; then, this value is nearly maintained for a relatively long time interval; after passing through the shear region, the value of γ_e is gradually increased to $\gamma_e \cong \gamma_{e0}$; once more, this property is consistent with the analogous property of the OT.

Relative Path Inclination. For model WS1, the relative path inclination γ of the GGT behaves in about the same way as the absolute path inclination γ_e; this property is consistent with the analogous property of the OT.

For models WS2 and WS3, the relative path inclination γ of the GGT is larger than the absolute path inclination γ_e; once more, this property is consistent with the analogous property of the OT.

Relative Velocity. For model WS2, the GGT exhibits a mild decrease in relative velocity; the velocity decrease ends at about the time when the downdraft ends; this property is consistent with the analogous property of the OT.

For models WS1 and WS3, the GGT exhibits a stronger decrease in relative velocity; the maximum drop in relative velocity depends mainly on the wind velocity difference ΔW_x and occurs at about the time when the shear ends; once more, this property is consistent with the analogous property of the OT.

5.8. Comment. From the present study of gamma guidance trajectories (Fig. 5) as well as from previous studies (Refs. 4-5), the following conclusions can be inferred. For weak-to-moderate shear/downdraft combinations, the GGT is characterized by a monotonic climb. For severe shear/downdraft combinations, the GGT is characterized by an initial climb, followed by nearly-horizontal flight, followed by renewed climbing after the aircraft has passed through the shear region. These properties are consistent with the analogous properties of the OT.

6. Conclusions

This paper is concerned with guidance strategies for near-optimum performance in a windshear. The take-off problem is considered with reference to flight in a vertical plane. In addition to the horizontal shear, the presence of a downdraft is assumed.

First, trajectories for optimum performance in a windshear are determined for different windshear models and different windshear intensities. Use is made of the methods of optimal control theory in conjunction with the dual sequential gradient-restoration algorithm (DSGRA) for optimal control problems. In this approach, global information on the wind flow field is needed.

Numerical experiments with the optimal control approach lead to the following conclusions: (i) for weak-to-moderate shear/downdraft combinations, the optimal trajectory is characterized by a monotonic climb; and (ii) for severe shear/downdraft combinations, the optimal trajectory is characterized by an initial climb, followed by nearly-horizontal flight, followed by renewed climbing after the aircraft has passed through the shear region.

Then, guidance strategies for near-optimum performance in a windshear are developed, starting from the optimal trajectories. Specifically, three guidance schemes are presented: an absolute gamma guidance scheme, based on the absolute path inclination; a relative gamma guidance scheme, based on the relative path inclination;and a theta guidance scheme, based on the pitch attitude angle. In this approach, local information on the wind flow field is needed.

Numerical experiments with the gamma/theta guidance schemes show that these schemes preserve properties (i) and (ii) of the optimal trajectories. Not only the resulting trajectories are close to the optimum trajectories, but they are considerably superior to the trajectories arising from alternative guidance schemes.

An important characteristic of the gamma/theta guidance schemes is their simplicity. Indeed, these guidance schemes are implementable using available instrumentation and/or modification of available instrumentation.

References

1. MIELE, A., WANG, T., and MELVIN, W. W., Optimal Flight Trajectories in the Presence of Windshear, Parts 1-4, Rice University, Aero-Astronautics Reports Nos. 191-194, 1985.
2. MIELE, A., Summary Report on NASA Grant No. NAG-1-516, Optimal Flight Trajectories in the Presence of Windshear, 1984-85, Rice University, Aero-Astronautics Report No. 195, 1985.
3. MIELE, A., WANG, T., and MELVIN, W. W., Optimal Take-Off Trajectories in the Presence of Windshear, Journal of Optimization Theory and Applications, Vol. 49, No. 1, pp. 1-45, 1986.
4. MIELE, A., WANG, T., and MELVIN, W. W., Guidance Strategies for Near-Optimum Performance in a Windshear, Parts 1-2, Rice University, Aero-Astronautics Reports Nos. 201-202, 1986.
5. MIELE, A., WANG, T., and MELVIN, W. W., Guidance Strategies for Near-Optimum Take-Off Performance in a Windshear, Journal of Optimization Theory and Applications, Vol. 50, No. 1, pp. 1-47, 1986.
6. ANONYMOUS, N. N., Low Altitude Windshear and Its Hazard to Aviation, National Academy Press, Washington, DC, 1983.
7. MIELE, A., Flight Mechanics, Vol. 1, Theory of Flight Paths, Addison-Wesley Publishing Company, Reading, Massachusetts, 1962.
8. FROST, W., and CROSBY, B., Investigations of Simulated Aircraft Flight through Thunderstorm Outflows, NASA, Contractor Report No. 3052, 1978.

9. MCCARTHY, J., BLICK, E. F., and BENSCH, R. R., Jet Transport Performance in Thunderstorm Windshear Conditions, NASA,Contractor Report No. 3207, 1979.

10. PSIAKI, M. L., and STENGEL, R. F., Analysis of Aircraft Control Strategies for Microbust Encounter, Paper No. AIAA-84-0238, AIAA 22nd Aerospace Sciences Meeting, Reno, Nevada, 1984.

11. FROST, W., and BOWLES, R. L., Windshear Terms in the Equations of Aircraft Motion, Journal of Aircraft, Vol. 21, No. 11, pp. 866-872, 1984.

12. ZHU,S. X., and ETKIN, B., Fluid-Dynamic Model of a Downburst, University of Toronto, Institute for Aerospace Studies, Report No. UTIAS-271, 1983.

13. ALEXANDER, M. B., and CAMP, D. W., Wind Speed and Direction Shears with Associated Vertical Motion during Strong Surface Winds, NASA, Technical Memorandum No. 82566, 1984.

14. FROST, W., CHANG, H. P., ELMORE, K. L., and MCCARTHY, J., Simulated Flight through JAWS Windshear: In-Depth Analysis Results, Paper No. AIAA-84-0276, AIAA 22nd Aerospace Sciences Meeting, Reno, Nevada, 1984.

15. CAMPBELL, C. W., A Spatial Model of Windshear and Turbulence for Flight Simulation, NASA, Technical Paper No. 2313, 1984.

16. ANONYMOUS, N. N., Flight Path Control in Windshear, Boeing Airliner, pp. 1-12, January-March 1985.

17. LEITMANN, G., The Calculus of Variations and Optimal Control, Plenum Publishing Corporation, New York, New York, 1981.

18. MIELE, A., PRITCHARD, R. E., and DAMOULAKIS, J. N., Sequential Gradient-Restoration Algorithm for Optimal Control Problems, Journal of Optimization Theory and Applications, Vol. 5, No. 4, pp. 235-282, 1970.

19. MIELE, A., DAMOULAKIS, J. N., CLOUTIER, J. R., and TIETZE, J. L., Sequential Gradient-Restoration Algorithm for Optimal Control Problems with Nondifferential Constraints, Journal of Optimization Theory and Applications, Vol. 13, No. 2, pp. 218-255, 1974.

20. MIELE, A., Recent Advances in Gradient Algorithms for Optimal Control Problems, Journal of Optimization Theory and Applications, Vol. 17, Nos. 5/6, pp. 361-430, 1975.

21. GONZALEZ, S., and MIELE, A., Sequential Gradient-Restoration Algorithm for Optimal Control Problems with General Boundary Conditions, Journal of Optimization Theory and Applications, Vol. 26, No. 3, pp. 395-425, 1978.

22. MIELE, A., Gradient Algorithms for the Optimization of Dynamic Systems, Control and Dynamic Systems, Advances in Theory and Application, Edited by C. T. Leondes, Academic Press, New York, New York, Vol. 16, pp. 1-52, 1980.

23. MIELE, A., and WANG, T., Primal-Dual Properties of Sequential Gradient-Restoration Algorithms for Optimal Control Problems, Part 1: Basic Problem, Rice University, Aero-Astronautics Report No. 183, 1985.

24. MIELE, A., and WANG, T., Primal-Dual Properties of Sequential Gradient-Restoration Algorithms for Optimal Control Problems, Part 2: General Problem, Rice University, Aero-Astronautics Report No. 184, 1985.

25. JOHNSON, C. D., Optimal Control with Chebyshev Minimax Performance Index, Journal of Basic Engineering, Vol. 89, No. 2, pp. 251-262, 1967.

26. MICHAEL, G. J., Computation of Chebyshev Optimal Control, AIAA Journal, Vol. 9, No. 5, pp. 973-975, 1971.

27. WARGA, J., Minimax Problems and Unilateral Curves in the Calculus of Variations, SIAM Journal on Control, Vol. 3, No. 1, pp. 91-105, 1965.

28. POWERS, W. F., A Chebyshev Minimax Technique Oriented to Aerospace Trajectory Optimization Problems, AIAA Journal, Vol. 10, No. 10, pp. 1291-1296, 1972.

29. HOLMAKER, K., A Minimax Optimal Control Problem, Journal of Optimization Theory and Applications, Vol. 28, No. 3, pp. 391-410, 1979.

30. HOLMAKER, K., A Property of an Autonomous Minimax Optimal Control Problem, Journal of Optimization Theory and Applications, Vol. 32, No. 1, pp. 81-87, 1980.

31. MIELE, A., MOHANTY, B. P., VENKATARAMAN, P., and KUO, Y. M., Numerical Solution of Minimax Problems of Optimal Control, Part 1, Journal of Optimization Theory and Applications, Vol. 38, No. 1, pp. 97-109, 1982.

32. MIELE, A., MOHANTY, B. P., VENKATARAMAN, P., and KUO, Y. M., Numerical Solution of Minimax Problems of Optimal Control, Part 2, Journal of Optimization Theory and Applications, Vol. 38, No. 1, pp. 111-135, 1982.

33. MIELE, A., and VENKATARAMAN, P., Optimal Trajectories for Aeroassisted Orbital Transfer, Acta Astronautica, Vol. 11, Nos. 7/8, pp. 423-433, 1984.

34. MIELE, A., and VENKATARAMAN, P., Minimax Optimal Control and Its Applications to the Reentry of a Space Glider, Recent Advances in the Aerospace Sciences, Edited by L. Casci, Plenum Publishing Corporation, New York, New York, pp. 21-40, 1985.

35. MIELE, A., and BASAPUR, V. K., Approximate Solutions to Minimax Optimal Control Problems for Aeroassisted Orbital Transfer, Acta Astronautica, Vol. 12, No. 10, pp. 809-818, 1985.

36. MIELE, A., BASAPUR, V. K., and MEASE, K. D., Nearly-Grazing Optimal Trajectories for Aeroassisted Orbital Transfer, Journal of the Astronautical Sciences, Vol. 34, No.1, pp. 3-18, 1986.

37. MIELE, A., and WANG, T., An Elementary Proof of a Functional Analysis Result Having Interest for Minimax Optimal Control of Aeroassisted Orbital Transfer Vehicles, Rice University, Aero-Astronautics Report No. 182, 1985.

38. COTTRELL, R. G., Optimal Intercept Guidance for Short-Range Tactical Missiles, IAAA Journal, Vol. 9, No. 7, pp. 1414-1415, 1971.

39. ASHER, R. B., and MATUZEWSKI, J. P., Optimal Guidance for Maneuvering Targets, Journal of Spacecraft and Rockets, Vol. 11, No. 3, pp. 204-206, 1974.

40. STENGEL, R. F., Optimal Guidance for the Space Shuttle Transition, Journal of Spacecraft and Rockets, Vol. 11, No. 3, pp. 173-179, 1974.

41. NAZAROFF, G. J., An Optimal Terminal Guidance Law, IEEE Transactions on Automatic Control, Vol. AC-21, No. 3, pp. 407-408, 1976.

42. GUELMAN, N., and SHINAR, J., Optimal Guidance Law in the Plane, Journal of Guidance, Control, and Dynamics, Vol. 7, No. 4, pp. 471-476, 1984.

List of Captions

Fig. 1. Coordinate systems and force diagram.

Fig. 2. Microburst encounter.

Fig. 3A. Wind velocity components W_x, W_h versus horizontal distance x.

Fig. 3B. Gradients of wind velocity components $\partial W_x/\partial x$, $\partial W_h/\partial x$ versus horizontal distance x.

Fig. 4A. Optimal trajectory: Wind velocity components W_x, W_h versus time t.

Fig. 4B. Optimal trajectory: Altitude h versus time t.

Fig. 4C. Optimal trajectory: Relative velocity V versus time t.

Fig. 4D. Optimal trajectory: Relative path inclination γ versus time t.

Fig. 4E. Optimal trajectory: Relative angle of attack α versus time t.

Fig. 4F. Optimal trajectory: Pitch attitude angle θ versus time t.

Fig. 4G. Optimal trajectory: Absolute path inclination γ_e versus time t.

Fig. 4H. Optimal trajectory: Energy per unit weight E versus time t.

Fig. 5A. Gamma guidance: Wind velocity components W_x, W_h versus time t.

Fig. 5B. Gamma guidance: Altitude h versus time t.

Fig. 5C. Gamma guidance: Relative velocity V versus time t.

Fig. 5D. Gamma guidance: Relative path inclination γ versus time t.

Fig. 5E. Gamma guidance: Relative angle of attack α versus time t.

Fig. 5F. Gamma guidance: Pitch attitude angle θ versus time t.

Fig. 5G. Gamma guidance: Absolute path inclination γ_e versus time t.

Fig. 5H. Gamma guidance: Energy per unit weight E versus time t.

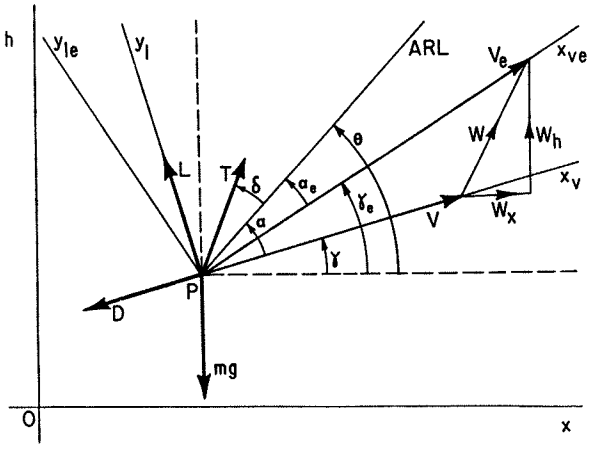

FIG. 1: COORDINATE SYSTEMS.

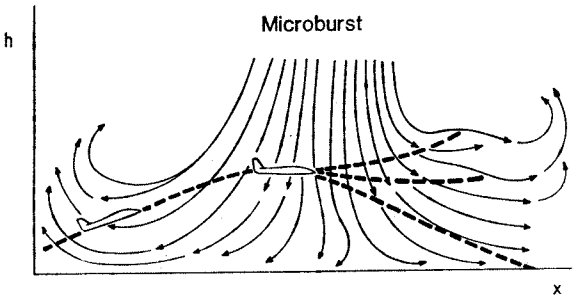

FIG. 2: MICROBURST ENCOUNTER.

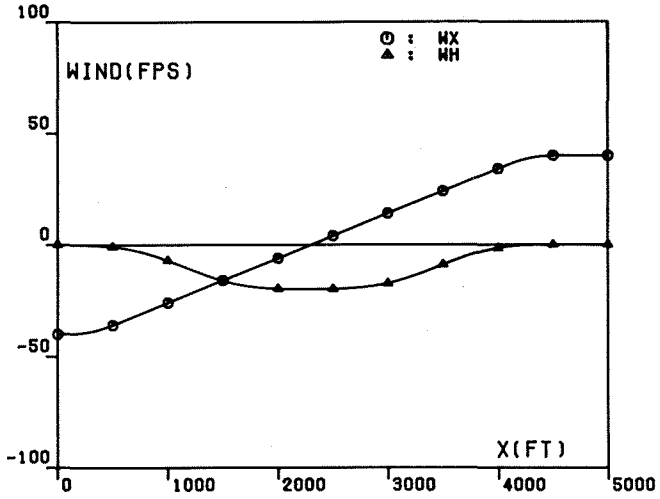

FIG.3A: WIND COMPONENTS.

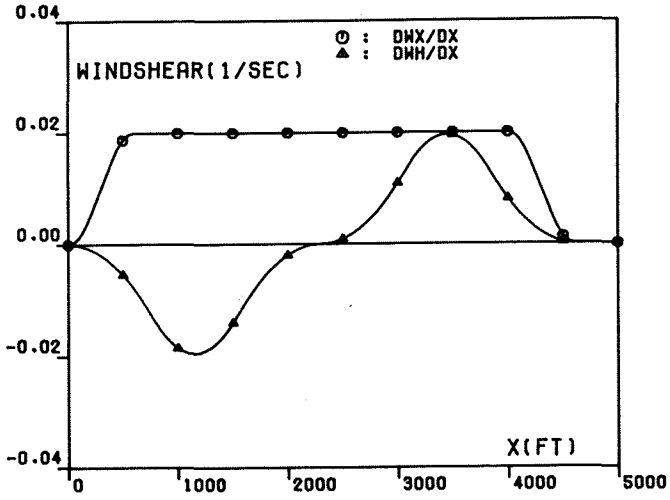

FIG.3B: GRADIENTS OF WIND COMPONENTS.

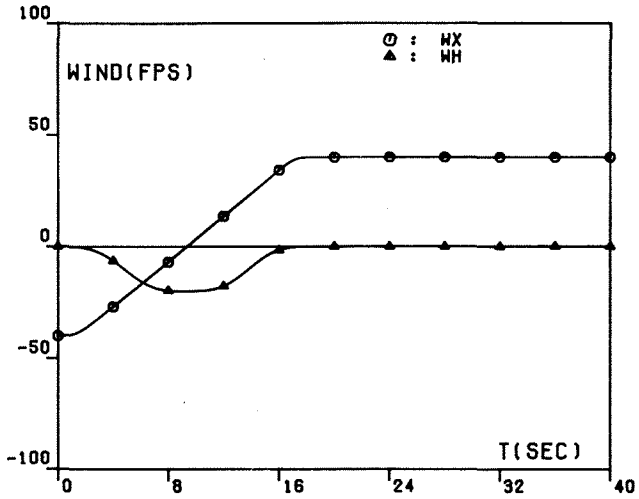

FIG.4A: OPTIMAL TRAJECTORY.

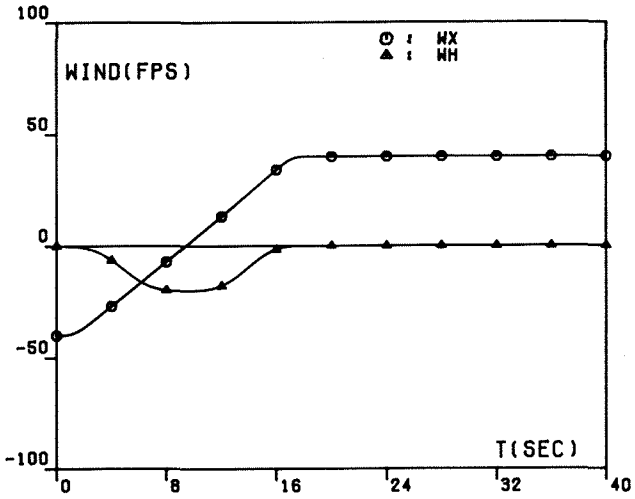

FIG.5A: GAMMA GUIDANCE.

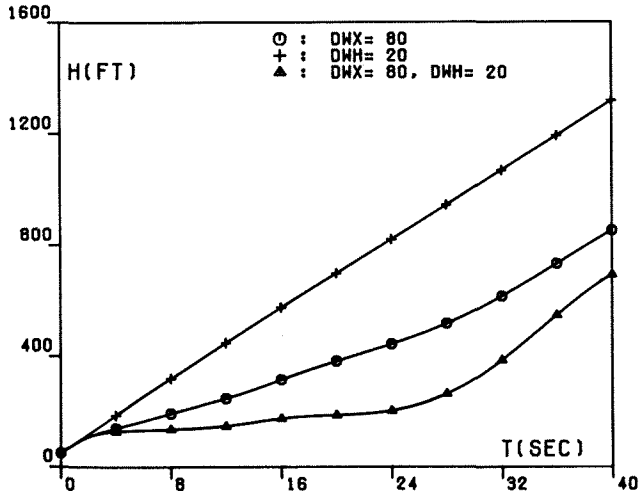

FIG.4B: OPTIMAL TRAJECTORY.

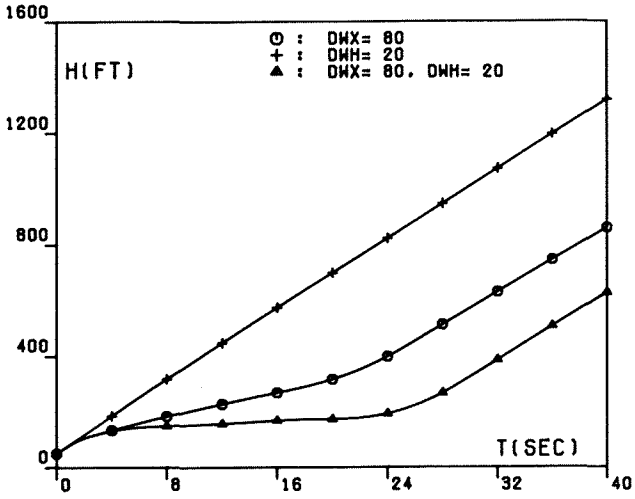

FIG.5B: GAMMA GUIDANCE.

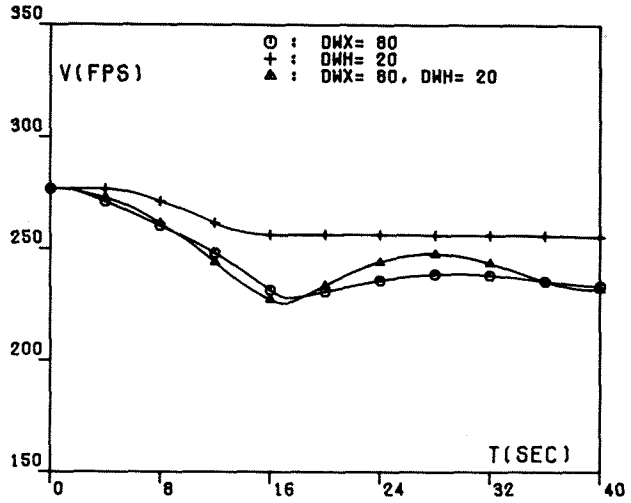

FIG.4C: OPTIMAL TRAJECTORY.

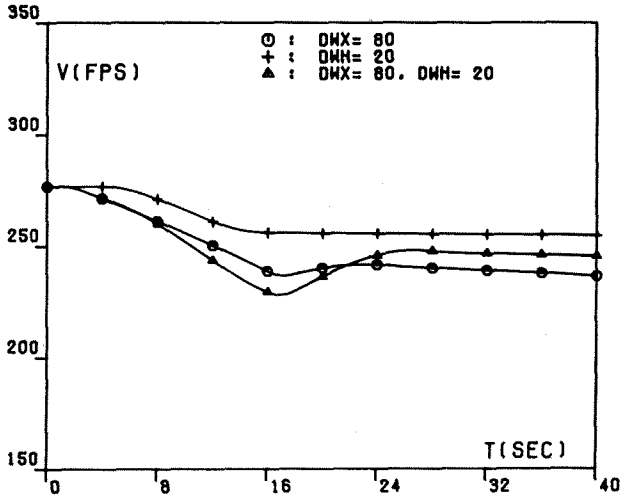

FIG.5C: GAMMA GUIDANCE.

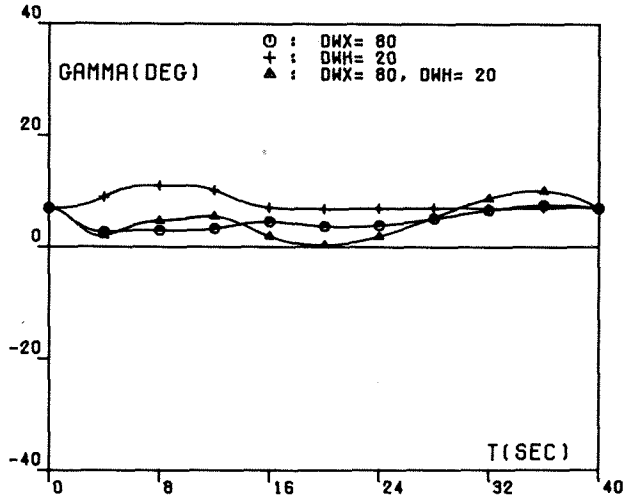

FIG.4D: OPTIMAL TRAJECTORY.

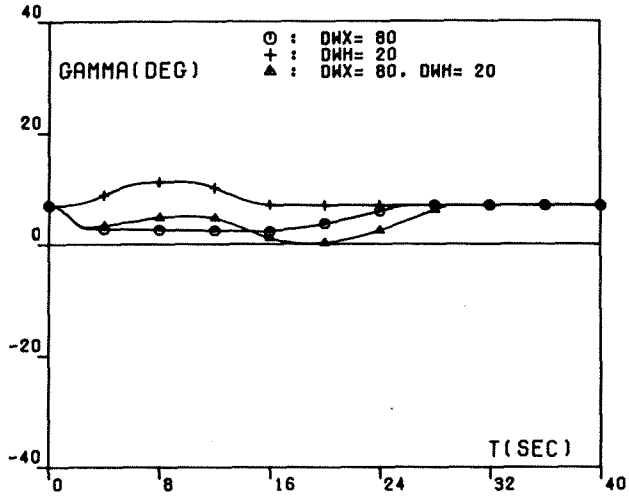

FIG.5D: GAMMA GUIDANCE.

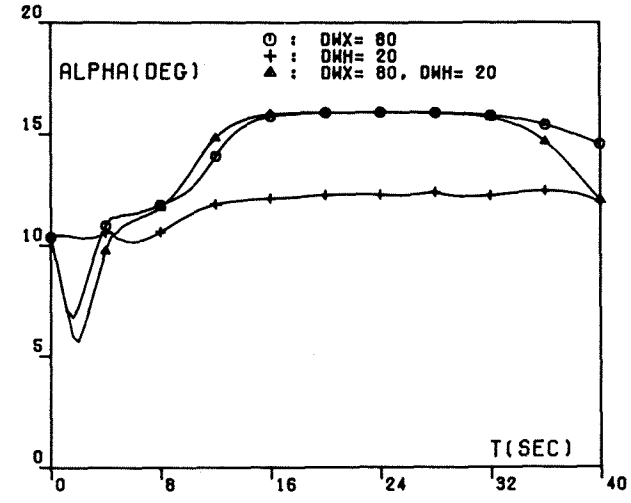

FIG.4E: OPTIMAL TRAJECTORY.

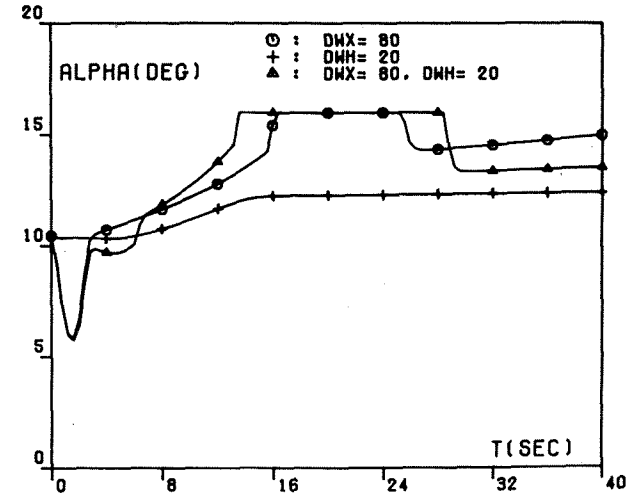

FIG.5E: GAMMA GUIDANCE.

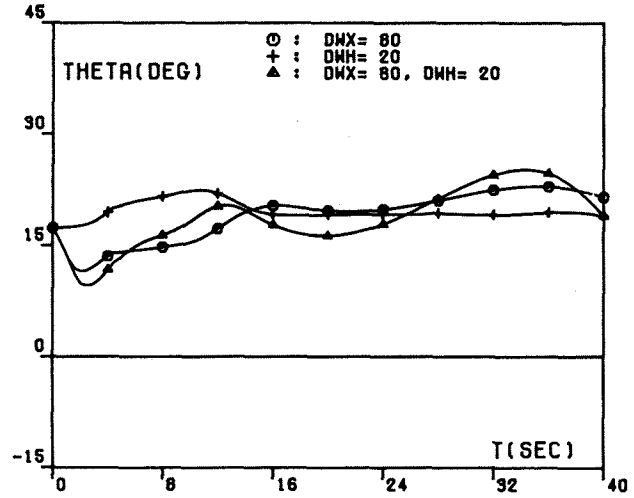

FIG.4F: OPTIMAL TRAJECTORY.

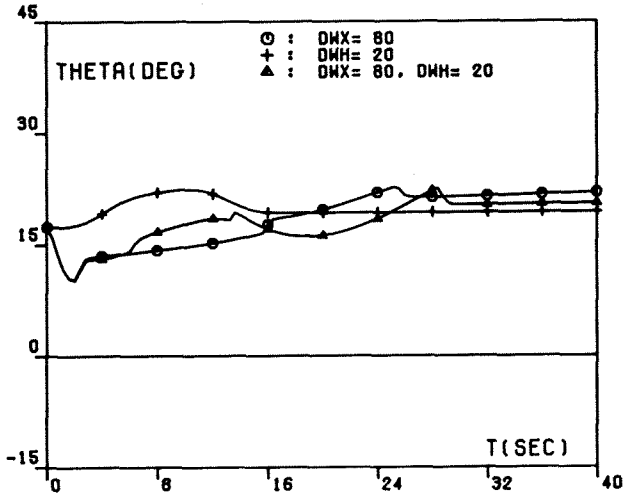

FIG.5F: GAMMA GUIDANCE.

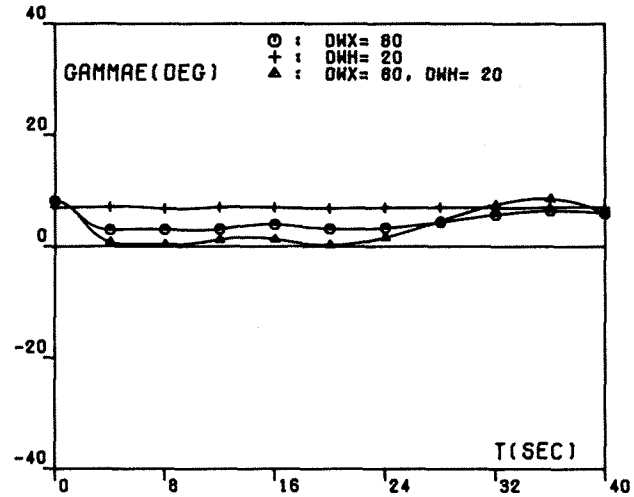

FIG.4G: OPTIMAL TRAJECTORY.

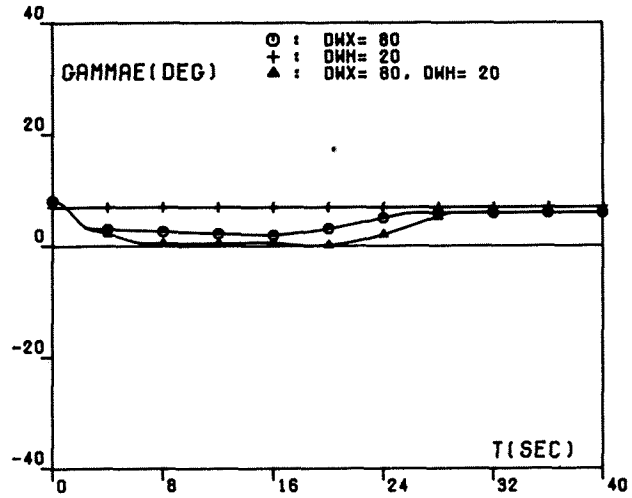

FIG.5G: GAMMA GUIDANCE.

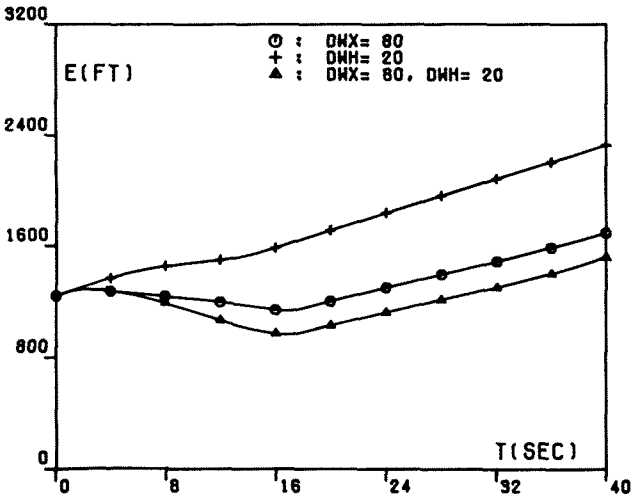

FIG.4H: OPTIMAL TRAJECTORY.

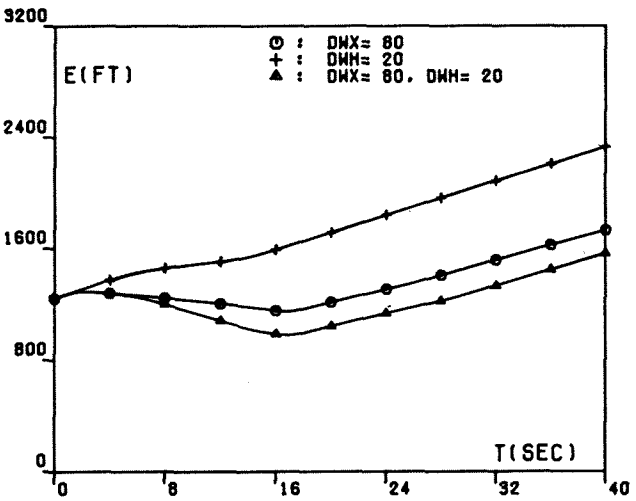

FIG.5H: GAMMA GUIDANCE.